

Two Layers of Computational Screening on Silaborane-based Clusters Filter $\text{Ca}(\text{SiB}_{11}\text{H}_{11}\text{CH}_3)_2$ as the Promising Electrolyte for Calcium-Ion Batteries

Abhiruchi Sharma,^[a] Anson Thomas,^[a] and Puneet Gupta^{*[a]}

Dedicated to Professor Rabindranath Mukherjee on the occasion of his 70th birthday

Calcium-ion batteries (CIBs) are promising energy storage systems, but the unavailability of adept electrolytes has hindered their development. In this work, a range of silaborane clusters ($\text{SiB}_{n-1}\text{H}_n^-$; $n=5-15$) were investigated using density functional theory (DFT) at $\omega\text{B97XD3}/6-311+\text{G(d,p)}$ level of theory. The vertical detachment energy (VDE), electrochemical stability window (ESW) and binding energy (BE) of the silaboranes were computed at the same level of DFT. A methodology based on molecular electrostatic potential surface analysis was designed to locate the most suitable binding site for calcium ions on the clusters. DFT results show that the

$\text{SiB}_{11}\text{H}_{12}^-$ cluster turns out to be superior to other candidates. Effect of substitution on silaboranes ($\text{SiB}_{n-1}\text{H}_{n-1}\text{R}^-$ $\text{R}=-\text{CH}_3$, $-\text{NCS}$, $-\text{CF}_3$, $-\text{F}$ and $-\text{Cl}$) was computed. $-\text{NCS}$ and $-\text{CF}_3$ substituted $\text{SiB}_{11}\text{H}_{12}^-$ ions were found to be the best from DFT. *Ab initio* molecular dynamics (AIMD) studies were performed to explore the interactions between silaborane-based electrolytes and the Ca anode. AIMD results highlight the decomposition of $-\text{NCS}$ and $-\text{CF}_3$ substituted $\text{SiB}_{11}\text{H}_{12}^-$ on Ca anode. DFT and AIMD studies reveal that $-\text{CH}_3$ substituted silaborane-based Ca-salt ($\text{Ca}(\text{SiB}_{11}\text{H}_{11}\text{CH}_3)_2$) is the promising electrolyte for CIBs.

Introduction

Lithium-ion batteries (LIBs) have dominated the realm of energy technology since their revolutionary development and commercialization in the 1990s.^[1-3] Nevertheless, the limited sources of raw materials for LIBs, the formation of hazardous dendrites, and the increasing cost of Li are the matters of great concern that call for developing new and better battery technologies.^[4] In this direction, the multivalent ion batteries (such as Mg^{2+} , Ca^{2+} , Zn^{2+} , and Al^{3+}) have emerged as strong contenders that can usher in another revolution in energy storage technology.^[5-19] This is due to their numerous benefits, such as improved safety features, higher abundance, higher theoretical charge density, and larger volumetric and gravimetric capacities.^[20] Calcium, the fifth most plentiful element in the Earth's crust, stands out as a highly potential candidate for the application in multivalent ion batteries.^[20,21] As an anode material, calcium provides a theoretical energy density of 2.06 Ah cm^{-3} , which is higher than that of graphite employed in contemporary LIBs (0.97 Ah cm^{-3}), and it possesses a lower standard redox potential of -2.87 V against SHE (Standard Hydrogen Electrode).^[22] The higher melting point of calcium (842°C) allows for safer operation at high temperatures. Moreover, a large number of calcium reserves and its low

cost would be an added advantage for the calcium-ion battery industry. Despite the many benefits of calcium, the absence of a suitable electrolyte has decelerated the progress in this field.^[23] The passivation layer formation in CIBs renders conventional salts unsuitable with calcium anode in aprotic solvents.^[24,25] Passivation is very prominent in CIBs because of the highly reducing nature of calcium.^[26] The passivation layer impedes the transport of calcium ions, thereby hampering the stripping/plating cycles. It is, therefore, imperative to design efficient electrolytes that either form a Ca-ion-permeable layer or mitigate the formation of a passivation layer altogether.^[6] Concerted efforts are being made with the ultimate goal of making CIBs commercially viable.^[27] Earlier efforts to develop liquid electrolytes for CIBs date back to the 1980s.^[28-31] In the last several years, numerous electrolytes based on salts such as $\text{Ca}(\text{ClO}_4)_2$, $\text{Ca}(\text{BF}_4)_2$, and $\text{Ca}(\text{TFSI})_2$ ($\text{TFSI}=\text{bis}(\text{trifluoromethanesulfonyl})\text{imide}$) have been meticulously explored for use in CIBs.^[32-34]

A quantum leap in the evolution of CIBs was reported in 2019 by the groups of Nazar and Zhao-Karger concurrently.^[26,35] The groups independently achieved reversible plating/stripping along with high anodic stability at room temperature using an electrolyte of bis-tetrakis(hexafluoroisopropoxy)borate ($\text{Ca}[\text{B}(\text{hfip})_4]_2$) salt having a weakly coordinating anion. The groups, however, reported insufficient cathodic stability and the formation of the CaF_2 passivation layer. The latter was attributed to the chemical reduction of the hexafluoroisopropoxy (hfip) ligand at the highly reducing Ca metal. The CaF_2 layer slows down the transport of calcium ions. Nevertheless, the understanding furnished by the partial success of ($\text{Ca}[\text{B}(\text{hfip})_4]_2$) salt points towards the utilization of weakly coordinating anions to design better CIBs. The weakly coordinating anions are, in general,

[a] M.Sc. A. Sharma, M.Sc. A. Thomas, Dr. P. Gupta
 Computational Catalysis Center, Department of Chemistry
 Indian Institute of Technology Roorkee
 Roorkee, Uttarakhand - 247667 (India)
 E-mail: puneet.gupta@cy.iitr.ac.in

 Supporting information for this article is available on the WWW under <https://doi.org/10.1002/batt.202300073>

chemically very stable, comparatively larger in size, and often lack donor atoms.^[36,37] All these characteristics work together to make it easier to detach the cation from the large anion, enhancing the ionic transport of cations through the electrolytic solution.^[28] The icosahedral monocarborane, $\text{CB}_{11}\text{H}_{12}^-$, is a classic example of weakly coordinating anions. Several metal salts with carboranes as anions have been extensively explored for the application in Li, Na, and Mg-ion batteries.^[38–44] Particularly, the weakly coordinating $\text{CB}_{11}\text{H}_{12}^-$ anion has a large electrochemical stability window and offers good reductive/oxidative stability. Hydrates based on $\text{CB}_{11}\text{H}_{12}^-$ anion have also been studied as solid-state electrolytes for battery applications.^[45] Recent experimental findings show that the $\text{Ca}(\text{CB}_{11}\text{H}_{12})_2$ salt in a mixture of dimethoxyethane (DME) and tetrahydrofuran (THF) solvents is a promising electrolyte for CIBs.^[46] The electrolyte displays an ionic conductivity of 4 mS cm^{-1} besides showing a wide electrochemical stability window (4 V vs. Ca^{2+}/Ca).^[46] The electrolyte also facilitates reversible plating/stripping at room temperature.

As of now, electrolytes based on carboranes of varying sizes have been investigated for application in alkali-ion batteries (such as LIBs), but they are yet to be explored for Ca-ion batteries.^[44,47] Besides carboranes ($\text{CB}_{n-1}\text{H}_n^-$), examining the properties of their silicon analogs ($\text{SiB}_{n-1}\text{H}_n^-$) also appears to be intriguing because the inclusion of the bigger silicon atom may expand the overall size of the anion. The larger size of silaboranes may lead to easier detachment of the metal ion from the anion, thereby enhancing the ionic conductivity.^[4,47] Additionally, the characteristics of carboranes and silaboranes may be anticipated to be comparable since silicon and carbon are the members of the same group. However, there are only a few reports on the utilization of silaboranes as electrolytes in batteries.^[4,47] This study aims to explore silaboranes for application in CIBs. Hence, a range of stable carborane and silaborane anions [$\text{XB}_{n-1}\text{H}_n^-$ ($\text{X}=\text{C/Si}; n=5–15$)] were extensively studied and systematically compared with the help of DFT-based computations for application as non-aqueous liquid electrolytes in CIBs. Properties such as the vertical detachment energy (VDE), electrochemical stability window (ESW), and binding energy (BE) of calcium ion with the anions were calculated to probe their stabilities and ease of detachment of Ca-ion. The energies of HOMO (highest occupied molecular orbital) and LUMO (lowest unoccupied molecular orbital) were also computed for anions. Further, the hydrogen atoms attached to the silicon atoms in silaboranes were substituted by functional groups ($-\text{NCS}$, $-\text{CF}_3$, $-\text{F}$, $-\text{Cl}$, and $-\text{CH}_3$) to modulate VDE, ESW, and BE of silaboranes.

Investigating the interaction of electrolyte with the metal anodes is a promising approach to predict their stability/decomposition, possible decomposition pathways and products comprising the passivation layer and so on.^[48–53] Hence, *ab initio* molecular dynamics simulations of the electrolytes based on calcium salts of silaboranes over the Ca anode surface were carried out to explore the real-time behaviour of the electrolytes. The charge transfer from the Ca anode surface to electrolytes was probed to gain insights into the interactions between the salts and the anode with time and the decomposition of salts over the anode.

Results and Discussion

Optimized geometries of anions

The optimized geometries of $\text{XB}_{n-1}\text{H}_n^-$ anions ($n=5–15$; $\text{X}=\text{C/Si}$) are given in Figure 1. The structures of carborane anions ranging from CB_5H_5^- to $\text{CB}_{14}\text{H}_{15}^-$ are denoted by small letters (a–k) and corresponding silaboranes (SiB_5H_5^- to $\text{SiB}_{14}\text{H}_{15}^-$) are represented by capital letters (A–K). The optimized coordinates of all these structures are provided in Section S20 of the Supporting Information (SI).

The $\text{XB}_{n-1}\text{H}_n^-$ ($\text{X}=\text{C/Si}$) anions can be obtained by replacing one boron atom of the $\text{B}_{12}\text{H}_{12}^{2-}$ parent cage with a C atom for carboranes and a Si atom for silaboranes. It is noteworthy that any boron of the $\text{B}_{12}\text{H}_{12}^{2-}$ cluster can be replaced with C/Si leading to several possible isomers. For this study, the isomers with the highest stability, as mentioned in previous reports, were chosen for further analysis.^[54,55] With an aim to improve the properties (VDE, ESW, and BE) of silaboranes, the hydrogen atoms attached to the Si atoms in silaboranes were further substituted with five functional groups, i.e., $-\text{NCS}$, $-\text{CF}_3$, $-\text{F}$, $-\text{Cl}$, and $-\text{CH}_3$. Among these, $-\text{CH}_3$ is electron-donating while the remaining four ($-\text{NCS}$, $-\text{CF}_3$, $-\text{F}$, $-\text{Cl}$) are electron-withdrawing in nature (Figure 2). Also, the NCS group offers two possibilities of ligation with Si of the silaborane cluster, i.e., it can ligate through S or N. We investigated both cases and found that isothiocyanate derivative ($-\text{NCS}$) results in a symmetric and more stable anionic structure than thiocyanate ($-\text{SCN}$). For instance, $\text{SiB}_{11}\text{H}_{11}\text{NCS}^-$ is $14.92 \text{ kcal mol}^{-1}$ more stable and symmetric than $\text{SiB}_{11}\text{H}_{11}\text{SCN}^-$ (see Figure S9 under Section S15 in SI). This outcome is in line with previous literature also.^[56] Thus, $-\text{NCS}$ group was used as the substituent where Si of silaboranes binds to nitrogen atom. Substitution with all five functional group ($-\text{NCS}$, $-\text{CF}_3$, $-\text{F}$, $-\text{Cl}$, and $-\text{CH}_3$) was done on every member of the silaborane series. The optimized geometries of all the functionalized silaboranes, along with cartesian coordinates are provided in Section S21 of SI.

In the following sections, the VDE and ESW of all candidate anions are discussed, along with the influence of the substituents on these properties in silaboranes. Thereafter, the BE of Ca^{2+} ion with the cluster anions is explained in detail. These properties give insights into the electrochemical behaviour of the considered anions for use in CIBs.

Vertical detachment energy (VDE)

The vertical detachment energy is a measure of the stability of an anion. It is the energy needed to eliminate an electron from an anion without altering its geometry (i.e., no structural relaxation). A greater value of VDE indicates higher stability of the anion; therefore, candidate anions with higher VDEs can act as efficient electrolytes. The computed VDEs for carboranes and silaboranes are listed in Table 1 and the variation of VDE with size of carboranes and silaboranes is illustrated in Section S3 of the SI.

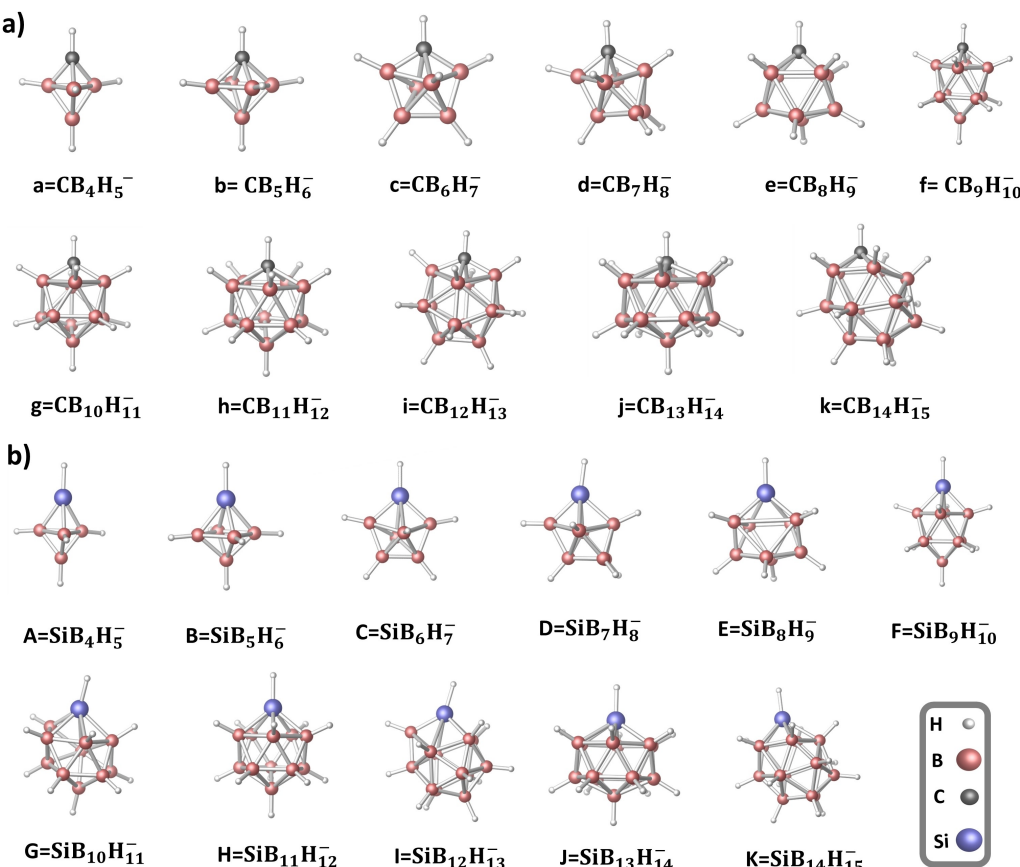


Figure 1. Optimized structures of a) $\text{CB}_{n-1}\text{H}_n^-$ and b) $\text{SiB}_{n-1}\text{H}_n^-$ anions at $\omega\text{B97XD3}/6-311+\text{G(d,p)}$ level of theory ($n=5-15$).

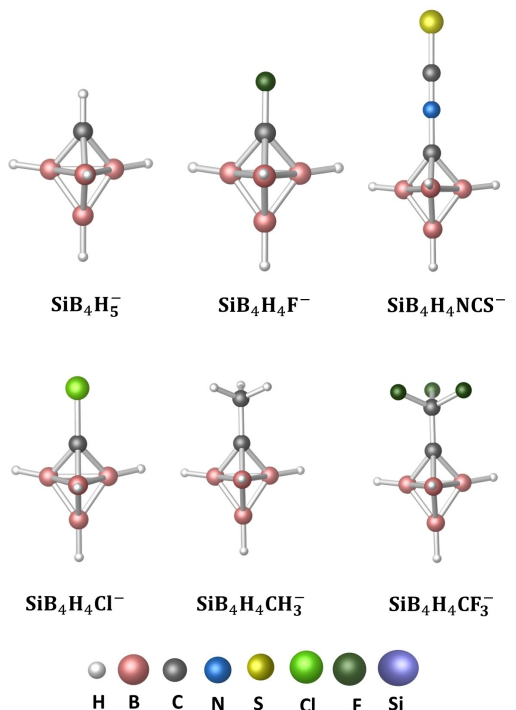


Figure 2. SiB_4H_5^- anion and the corresponding functionalized structures.

The calculated VDEs of carboranes and silaboranes are in close agreement with the VDEs reported by Kushwaha *et al.* for a similar set of carborane and silaborane anions.^[4] This validates the accuracy of the computational model and methods used in the present study. It can be seen from Table 1 that all the cluster anions apart from CB_4H_5^- (3.42 eV), SiB_4H_5^- (3.22 eV) and SiB_7H_8^- (3.51 eV), are superhalogens since their VDEs exceed the electron affinity of halogens (3.62 eV for chlorine).^[47,57,58]

The $\text{CB}_{11}\text{H}_{12}^-$ and $\text{SiB}_{11}\text{H}_{12}^-$ anions exhibit superior VDE than other candidates in their respective series (Table 1). These results are in line with previous works that reported higher stability of the $\text{XB}_{11}\text{H}_{12}^-$ anion ($\text{X}=\text{C/Si}$).^[4,44,59] The enhanced stability of $\text{XB}_{11}\text{H}_{12}^-$ ion is indissolubly associated with its high symmetry and an intense 3-dimensional aromatic character. The higher resonance stabilization in parent $\text{B}_{12}\text{H}_{12}^{2-}$ has been reported in previous literature as well.^[54] Another important observation is that the VDE values for silaboranes are found to be comparable to that of carboranes. For example, the VDE for SiB_4H_5^- (3.22 eV), SiB_7H_8^- (3.51 eV), and $\text{SiB}_{12}\text{H}_{13}^-$ (5.03 eV) are close to that of corresponding carboranes, i.e., CB_4H_5^- (3.42 eV), CB_7H_8^- (3.88 eV), and $\text{CB}_{12}\text{H}_{13}^-$ (5.28 eV). The meager difference in the VDE indicates that the silaboranes may act as promising electrolytes in CIBs. To augment the VDE of all the silaboranes, the H atoms attached to the Si atoms were replaced with five different functional groups ($-\text{F}$, $-\text{Cl}$, $-\text{CF}_3$, $-\text{CH}_3$ and $-\text{NCS}$). The variation in VDE of functionalized silaboranes with size is shown

Table 1. VDE (eV) of Carboranes and Silaboranes ($\text{CB}_{n-1}\text{H}_n^-$ and $\text{SiB}_{n-1}\text{H}_n^-$; $n=5-15$).

$\text{CB}_{n-1}\text{H}_n^-$	VDE [eV]	$\text{SiB}_{n-1}\text{H}_n^-$	VDE [eV]
CB_4H_5^-	3.42	SiB_4H_5^-	3.22
CB_5H_6^-	3.92	SiB_5H_6^-	4.20
CB_6H_7^-	4.24	SiB_6H_7^-	4.57
CB_7H_8^-	3.88	SiB_7H_8^-	3.51
CB_8H_9^-	4.28	SiB_8H_9^-	4.38
$\text{CB}_9\text{H}_{10}^-$	5.70	$\text{SiB}_9\text{H}_{10}^-$	4.59
$\text{CB}_{10}\text{H}_{11}^-$	4.69	$\text{SiB}_{10}\text{H}_{11}^-$	4.54
$\text{CB}_{11}\text{H}_{12}^-$	6.05	$\text{SiB}_{11}\text{H}_{12}^-$	6.01
$\text{CB}_{12}\text{H}_{13}^-$	5.28	$\text{SiB}_{12}\text{H}_{13}^-$	5.03
$\text{CB}_{13}\text{H}_{14}^-$	5.10	$\text{SiB}_{13}\text{H}_{14}^-$	5.40
$\text{CB}_{14}\text{H}_{15}^-$	5.30	$\text{SiB}_{14}\text{H}_{15}^-$	4.63

in Figure 3 and the corresponding VDE values are given in Section S4 of the SI.

The electron-withdrawing groups pull the electron density of the clusters toward themselves, and hence, the propensity of clusters to accept electrons increases, which amplifies the VDE values.^[60] In contrast, the electron-donating group ($-\text{CH}_3$) decreases the VDE values slightly. For most anions, it can be noted that $-\text{NCS}$ and $-\text{CF}_3$ increase the VDE values to the maximum extent, indicating greater stability of the clusters with these substituents. For instance, the VDE of $\text{SiB}_{11}\text{H}_{12}^-$ (H in Figure 3) after incorporating the $-\text{CF}_3$ group rises from 6.01 eV to 6.34 eV. The $-\text{CF}_3$ group provides a maximum increment in VDE followed by $-\text{NCS}$, establishing that substitution with these functional groups enhances the stability of the anions. It can also be noted that in silaboranes, the overall trend of VDE variation with the cluster size remains the same irrespective of the substituent incorporated (Figure 3).

Further, it is interesting to see that the VDE values are generally higher for larger clusters due to the greater delocalization of the negative charge. This is consistent with the widely acknowledged observation that the stabilities of these clusters

generally increase as the number of vertices increases.^[54] However, this increase in VDE follows a zig-zag trend (cf. Table 1 and Figure S3 in the SI). For instance, the VDE values increase from SiB_4H_5^- (3.22 eV) to SiB_6H_7^- (4.57 eV) followed by a decrease at SiB_7H_8^- (3.51 eV) and then increases again. This irregularity in VDE can be understood on the basis of the 3-dimensional aromaticity of the cluster anions quantified in terms of nuclear independent chemical shift (NICS) at the geometrical centres of the cluster ions. The NICS values can be regarded as another measure of the stability of cluster anions. The more negative the NICS, the greater the aromaticity and stability.^[54] The NICS values of the silaborane anions were calculated and are provided in Section S5, and the variation of NICS with the size of silaboranes is shown in Section S6 of the SI. On carefully observing the stability trend obtained from NICS analysis, it is found that the trend is almost similar to the stability pattern from VDE calculations. The resemblance in the NICS and VDE variation with silaborane size to an appreciable extent indicates that aromaticity plays a significant role in governing the overall VDE of anions. Thus, the NICS values account for the irregular trends in the VDE. The VDE analysis, therefore, gives an idea about the stability of the considered cluster anions for their application in CIBs.

Electrochemical stability window (ESW)

Another important design criterion for a suitable electrolyte is a wide electrochemical stability window.^[58,61] The ESW of an anion is indicative of the potential window in which the anion is neither oxidized nor reduced; thus, the anions with larger ESW values act as more suitable electrolytes. The HOMO-LUMO gaps for carboranes and silaboranes with increasing cluster size are shown in Figure 4, and computed values of ESW of carboranes and silaboranes are provided in Table 2. Further, the energies of HOMO and LUMO and the cathodic-anodic limits of all

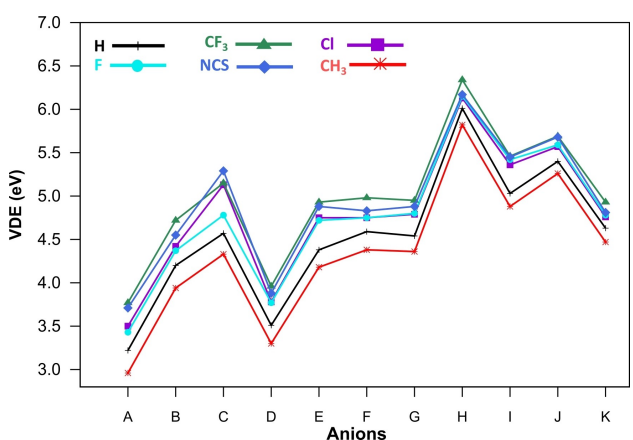


Figure 3. Variation in VDE of functionalized silaborane anions with cluster size (where A–K denote the $\text{SiB}_{n-1}\text{H}_{n-1}\text{R}^-$ ions; R = $-\text{H}$, $-\text{Cl}$, $-\text{F}$, $-\text{CF}_3$, $-\text{NCS}$ and $-\text{CH}_3$; n = 5–15).

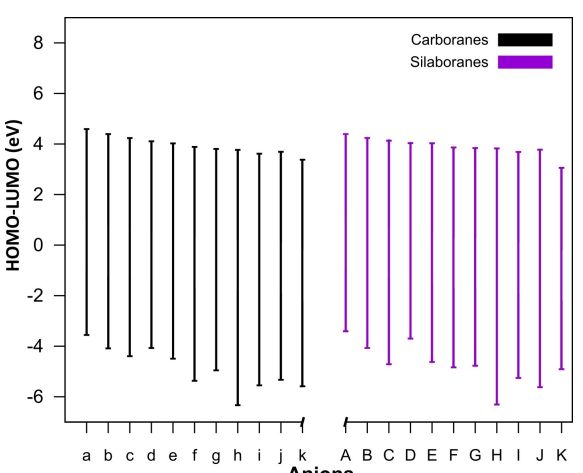


Figure 4. The HOMO-LUMO gap for carboranes and silaboranes (where small letters a–k denote $\text{CB}_{n-1}\text{H}_n^-$ ions, and capital letters A–K represent $\text{SiB}_{n-1}\text{H}_n^-$ ions; n = 5–15; the upper limits represent the energies of LUMO, while the lower limits correspond to the energies of HOMO).

Table 2. ESW (V) of Carboranes and Silaboranes ($\text{CB}_{n-1}\text{H}_n^-$ and $\text{SiB}_{n-1}\text{H}_n^-$; $n=5-15$).

$\text{CB}_{n-1}\text{H}_n^-$	ESW [V]	$\text{SiB}_{n-1}\text{H}_n^-$	ESW [V]
CB_4H_5^-	8.15	SiB_4H_5^-	7.80
CB_5H_6^-	8.48	SiB_5H_6^-	8.31
CB_6H_7^-	8.63	SiB_6H_7^-	8.85
CB_7H_8^-	8.18	SiB_7H_8^-	7.73
CB_8H_9^-	8.52	SiB_8H_9^-	8.65
$\text{CB}_9\text{H}_{10}^-$	9.26	$\text{SiB}_9\text{H}_{10}^-$	8.70
$\text{CB}_{10}\text{H}_{11}^-$	8.76	$\text{SiB}_{10}\text{H}_{11}^-$	8.61
$\text{CB}_{11}\text{H}_{12}^-$	10.10	$\text{SiB}_{11}\text{H}_{12}^-$	10.13
$\text{CB}_{12}\text{H}_{13}^-$	9.17	$\text{SiB}_{12}\text{H}_{13}^-$	8.94
$\text{CB}_{13}\text{H}_{14}^-$	9.02	$\text{SiB}_{13}\text{H}_{14}^-$	9.40
$\text{CB}_{14}\text{H}_{15}^-$	8.96	$\text{SiB}_{14}\text{H}_{15}^-$	7.97

unsubstituted anions are given in Section S7 of the SI. The ESW values of carboranes and silaboranes lie between 7.5 V to 10.5 V (Table 2). From Figure 4, it is seen that the electrochemical window is greater for larger-sized anions in most cases due to the superior stabilization provided by the greater delocalization of negative charge. Further, $\text{CB}_{11}\text{H}_{12}^-$ (10.10 V; H in Figure 4) and $\text{SiB}_{11}\text{H}_{12}^-$ (10.13 V; H in Figure 4) anions distinctly exhibit maximum ESW in their respective groups. This is consistent with the previous reports emphasizing the greater ESW for $\text{XB}_{11}\text{H}_{12}^-$ ions ($X=\text{C/Si}$).^[4]

Another interesting observation is that the ESWs of silaboranes are quite close to that of carboranes. In some cases, the ESW values of silaboranes are lower than the analogous carboranes. For instance, the ESW of SiB_7H_8^- , $\text{SiB}_{12}\text{H}_{13}^-$ and $\text{SiB}_9\text{H}_{10}^-$ are 0.45, 0.23 and 0.56 V smaller than corresponding carboranes, i.e., CB_7H_8^- , $\text{CB}_{12}\text{H}_{13}^-$, and $\text{CB}_9\text{H}_{10}^-$, respectively. Thus, the ESW values of functionalized silaboranes were also calculated. The variation in ESW of substituted silaboranes with size is illustrated in Figure 5 and corresponding ESW values are given in Section S8 of the SI. The energies of HOMO and LUMO and the cathodic-anodic limits of all substituted silaborane anions are given in Section S9 of the SI. It can be noted from Figure 5 that the silaboranes with $-F$, $-Cl$, $-CF_3$, and $-NCS$ substituents show comparatively higher ESW than the corresponding non-functionalized anions. On the other hand, the $-CH_3$ group decreases the ESW width. The electron-pulling groups stabilize the HOMO which in turn widens the stability window. Also, for most scenarios, $-CF_3$ attachment provides maximum ESW width followed by the $-NCS$ and $-F$.

This suggests better performance of silaboranes with these substituents ($-CF_3$ and $-NCS$) in CIBs. For example, the ESW of $\text{SiB}_{11}\text{H}_{12}^-$ (cf. H in Figure 5 and Section S8 of the SI) rises from 10.13 V to 10.62 V on replacing the hydrogen by $-CF_3$ group. Hence, the ESW for silaboranes are comparable to that of corresponding carboranes highlighting the potential of silaboranes as good alternatives to carboranes for application in CIBs.

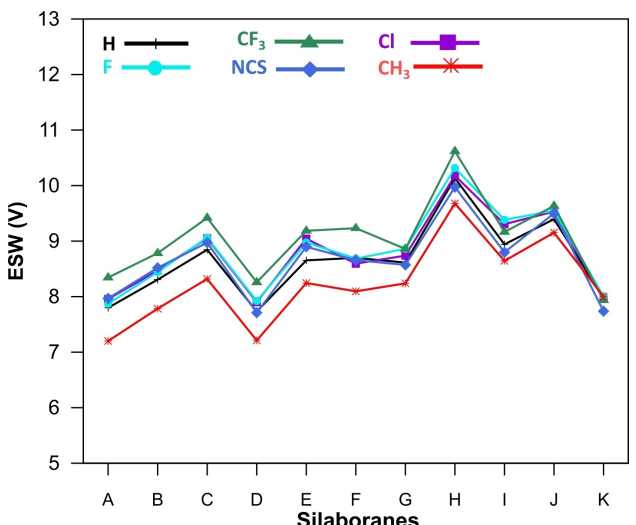


Figure 5. The variation in the ESW of functionalized silaboranes with size (where capital letters A–K represent $\text{SiB}_{n-1}\text{H}_{n-1}\text{R}^-$ ions; R = $-H$, $-F$, $-Cl$, $-CF_3$ and $-NCS$; $n=5-15$).

Binding energy (BE)

Understanding the atomic level interactions between the metal cation and the anion can give fruitful insights into the ease with which metal is detached from the anion during battery operation. The strength of this interaction can be quantified in terms of binding energy of the metal cation ($\Delta E_{\text{Ca}}^{2+}$) with the anion. A greater binding energy between the metal cation and the anion indicates stronger binding between the two. This translates to more difficult detachment of metal from the anionic cluster. In other words, a suitable electrolyte is one with a lower binding energy value. The carborane/silaborane clusters offer many possible binding sites for calcium. Therefore, before evaluating the BE, the foremost task is to find the most favourable binding site of calcium on the cluster anion.

We started off by manually identifying all unique possible binding sites of calcium on the cluster and divided these sites into bridged and face-centered sites. The bridged binding sites represent the positions over the middle of a bond between two atoms, while the face-centred sites are the positions at the centre of a triangular face formed by three boron atoms, as shown in Figure 6(a). For example, the CB_4H_5^- anion offers five unique potential binding sites for metal ion (Figure 6b). Calcium was placed at different binding sites, and the resulting $\text{Ca}^{2+}/\text{CB}_{n-1}\text{H}_n^-$ ion-pairs were optimized to find the most stable position of calcium on the cluster. The best binding site is the one with the least energy. This strategy was utilized to get the most probable ion-pair for all unsubstituted carboranes. However, it was a tedious task to do for larger clusters. To overcome this issue, we have devised a computational technique based on the analysis of the molecular electrostatic potential (MESP) surface of the anions. Using the MESP surface, the most negative electrostatic potential (ESP) point was determined, and the Ca^{2+} ion was placed at these points. The resulting ion-pairs were then fully optimized.

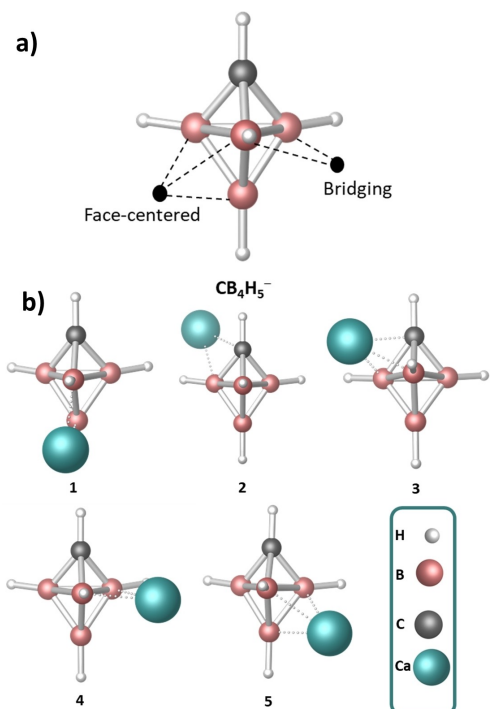


Figure 6. a) An illustration of bridging and face-centered binding sites and b) five possible unique binding sites of Ca^{2+} on CB_4H_5^- ion.

Interestingly, the position of calcium after optimization was identical to the most stable position found by manually placing calcium at all unique binding sites. This validates the robustness of this methodology, illustrated in Figure 7. The prediction of cation binding site on cluster using the MESP method is quite accurate, and the results are in complete agreement with the experimental studies. For $\text{CB}_{11}\text{H}_{12}^-$ anion, it is known in literature that the cation prefers to bind to the bottom most sites with respect to carbon atom.^[62] Our MESP approach also provided the same outcome (h' in Figure 8) further validating the effectiveness of this method. Also, it is important to highlight that there are many possible metastable states where calcium may bind to different positions other than the one found using MESP. However, the difference in energies of the metastable states from the most stable states is not very high. The most

stable ion-pair was taken for further calculations to predict accurate trends in the binding energy variation (see Section S10 in SI for a more detailed discussion).

Thus, the MESP analysis can be a powerful tool for obtaining the preferred binding site for Ca^{2+} and was used for further calculations. The ion-pairs of the non-functionalized calcium-carboranes and calcium-silaboranes are illustrated in Figure 8. The optimized cartesian coordinates for all the unsubstituted ion-pairs are provided in the Section S22 of the SI. The variation in BE for the silaborane and carborane-based calcium ion-pairs with size is depicted in Figure 9 and the corresponding BE values are tabulated in Table 3. From Figure 9, it can be inferred that the BE values are generally lower for larger anion-based ion-pairs and vice-versa. Such a trend is an outcome of the higher size difference between the two binding species (Ca^{2+} cation and the anionic cluster) that decreases the binding efficiency (or binding energy) on moving towards larger clusters.

All BE values lie in the range of 10.00 eV–11.50 eV. Another interesting finding is that the BE values for $\text{Ca}^{2+}/\text{SiB}_{n-1}\text{H}_n^-$ ion-pairs are comparatively higher than the corresponding $\text{Ca}^{2+}/\text{CB}_{n-1}\text{H}_n^-$ ion-pairs (Figure 9; $n=5\text{--}15$). Incorporating a larger silicon atom increases the van der Waals (vdW) volume of the silaborane clusters to values higher than the corresponding carboranes,^[4] for instance, the vdW volume of the $\text{CB}_{11}\text{H}_{12}^-$ ion is 1547.93 Bohr³, while that of $\text{SiB}_{11}\text{H}_{12}^-$ is 1623.62 Bohr³. This suggests that the $\text{Ca}^{2+}/\text{SiB}_{n-1}\text{H}_n^-$ ion-pairs should possess less BE than analogous $\text{Ca}^{2+}/\text{CB}_{n-1}\text{H}_n^-$ ion-pairs, thereby facilitating the easier detachment of Ca^{2+} from silaboranes than carboranes.

However, an opposite trend is observed, that is, higher BE values are obtained for silaborane-based ion-pairs. This is a direct consequence of BE being dependent on more factors apart from size. For instance, the NPA (Natural Population Analysis) charges on boron atoms involved in binding with Ca^{2+} in the case of silaboranes (cf. Section S11 of the SI) are more negative than the corresponding carboranes. Thus, boron atoms in silaboranes bind the calcium ion more firmly than in carboranes. This factor appears to dominate over the size-dependency of BE, resulting in higher binding energies for silaboranes. This observation clarifies that there is no direct connection between the size of the anion and the binding

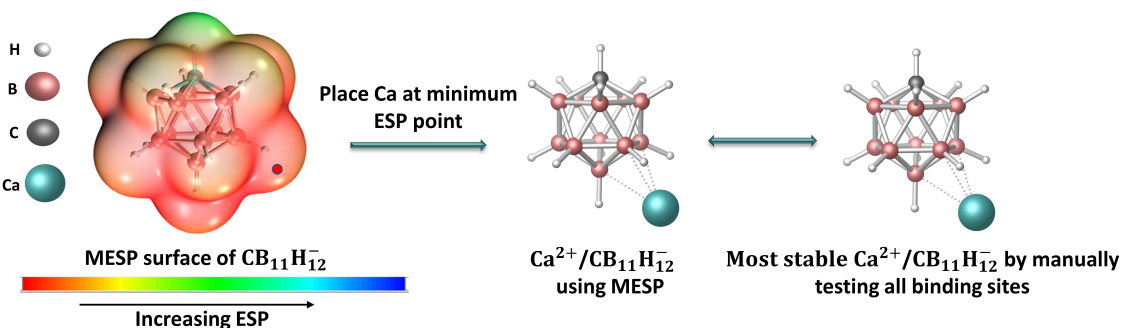


Figure 7. Placing Ca at the minimum ESP point (solid red circle) of the MESP surface (plotted at 0.001 a.u. isovalue) of $\text{CB}_{11}\text{H}_{12}^-$ ion gives the most stable binding site for Ca, as also determined by the manual technique.

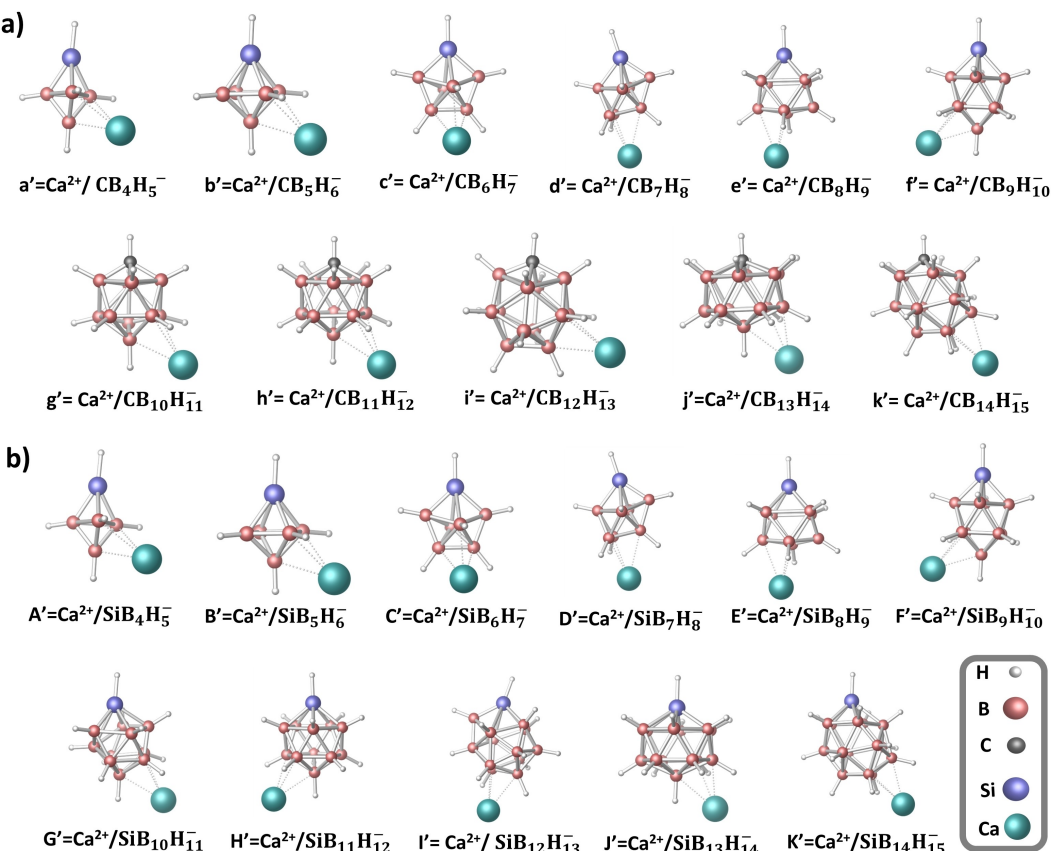


Figure 8. Optimized structures of $\text{Ca}^{2+}/\text{CB}_{n-1}\text{H}_n^-$ and $\text{Ca}^{2+}/\text{SiB}_{n-1}\text{H}_n^-$ ion-pairs at $\omega\text{B97XD3/6-311+G(d,p)}$ level of theory (where $a'-k'$ and $A'-K'$ represent $\text{Ca}^{2+}/\text{CB}_{n-1}\text{H}_n^-$ and $\text{Ca}^{2+}/\text{SiB}_{n-1}\text{H}_n^-$ ion-pairs respectively; $n=5-15$).

energy of the metal cation with the anion, indicating that many parameters influence the overall BE. Size is only one of the many factors governing the overall binding efficiency. Consequently, no regular decrease in BE is observed on moving toward larger clusters. The binding of metal cation with the negatively charged boron atoms of the carborane/silaborane clusters is well established in previous literature also.^[55,62]

The binding energies of calcium with functionalized silaborane anions were also calculated. The computed binding energies for all ion-pairs are tabulated in Section S12 of the SI. The optimized cartesian coordinates for all functionalized Ca-silaborane ion-pairs are given in Section S23 of the SI. The variation of BE with size for functionalized Ca-silaborane ion-pairs is illustrated in Figure 10. It can be noticed from Figure 10 that the BE for $-F$, $-Cl$, $-CF_3$, and $-NCS$ functionalized silaboranes, are slightly lower in magnitude than non-functionalized silaboranes, as electron-withdrawing groups reduce the effective negative charge on the anion cluster leading to less efficient binding with the metal cation. The BE of $\text{Ca}^{2+}/\text{SiB}_{11}\text{H}_{12}$ (H' in Figure 10) ion-pair decreases from 10.45 eV to 10.07 eV and 10.20 eV for $-CF_3$ and $-NCS$ substitutions, respectively. This signifies that electron withdrawing groups can bring down the BE of calcium-silaborane ion-pairs. Further, the $-\text{CH}_3$ group increases the BE of the ion-pairs. For instance, the BE of $\text{Ca}^{2+}/\text{SiB}_{11}\text{H}_{11}\text{CH}_3$ (H' in Figure 10) is found to be 10.66 eV, which is larger than the corresponding non-functionalized (10.45 eV for $\text{Ca}^{2+}/\text{SiB}_{11}\text{H}_{12}$) ion-pair. These results indicate that substitution with $-CF_3$ and $-NCS$ groups may lead to easier detachment of calcium ion from the cluster, enhancing the overall electrochemical properties by increasing the ionic mobility. The high VDE and ESW and low BE of the $-CF_3$ and $-NCS$ substituted $\text{SiB}_{11}\text{H}_{12}^-$ anions collectively indicate that the corresponding

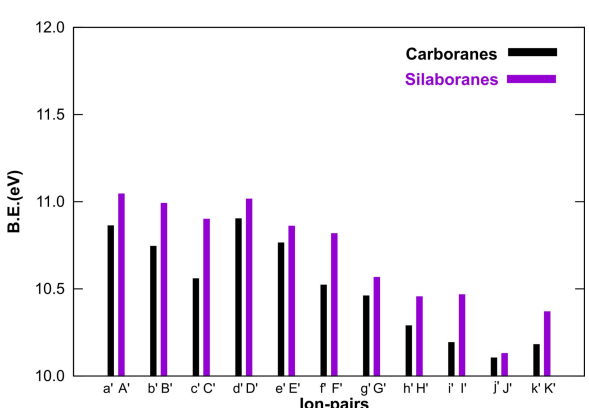


Figure 9. The variation in BE of unsubstituted calcium-carborane and calcium-silaborane ion-pairs with size (where $a'-k'$ denote the $\text{Ca}^{2+}/\text{CB}_{n-1}\text{H}_n^-$ ion-pairs and $A'-K'$ denote the $\text{Ca}^{2+}/\text{SiB}_{n-1}\text{H}_n^-$ ion-pairs; $n=5-15$).

Table 3. Binding energies of carborane and silaborane-based ion-pairs.

$\text{Ca}^{2+}/\text{CB}_{n-1}\text{H}_n^-$	BE [eV]	$\text{Ca}^{2+}/\text{SiB}_{n-1}\text{H}_n^-$	BE [eV]
$\text{Ca}^{2+}/\text{CB}_4\text{H}_5^-$	10.86	$\text{Ca}^{2+}/\text{SiB}_4\text{H}_5^-$	11.04
$\text{Ca}^{2+}/\text{CB}_5\text{H}_6^-$	10.74	$\text{Ca}^{2+}/\text{SiB}_5\text{H}_6^-$	10.99
$\text{Ca}^{2+}/\text{CB}_6\text{H}_7^-$	10.56	$\text{Ca}^{2+}/\text{SiB}_6\text{H}_7^-$	10.90
$\text{Ca}^{2+}/\text{CB}_7\text{H}_8^-$	10.90	$\text{Ca}^{2+}/\text{SiB}_7\text{H}_8^-$	11.01
$\text{Ca}^{2+}/\text{CB}_8\text{H}_9^-$	10.76	$\text{Ca}^{2+}/\text{SiB}_8\text{H}_9^-$	10.86
$\text{Ca}^{2+}/\text{CB}_9\text{H}_{10}^-$	10.52	$\text{Ca}^{2+}/\text{SiB}_9\text{H}_{10}^-$	10.82
$\text{Ca}^{2+}/\text{CB}_{10}\text{H}_{11}^-$	10.46	$\text{Ca}^{2+}/\text{SiB}_{10}\text{H}_{11}^-$	10.56
$\text{Ca}^{2+}/\text{CB}_{11}\text{H}_{12}^-$	10.29	$\text{Ca}^{2+}/\text{SiB}_{11}\text{H}_{12}^-$	10.45
$\text{Ca}^{2+}/\text{CB}_{12}\text{H}_{13}^-$	10.19	$\text{Ca}^{2+}/\text{SiB}_{12}\text{H}_{13}^-$	10.47
$\text{Ca}^{2+}/\text{CB}_{13}\text{H}_{14}^-$	10.10	$\text{Ca}^{2+}/\text{SiB}_{13}\text{H}_{14}^-$	10.13
$\text{Ca}^{2+}/\text{CB}_{14}\text{H}_{15}^-$	10.18	$\text{Ca}^{2+}/\text{SiB}_{14}\text{H}_{15}^-$	10.37

calcium salts may be better CIB electrolytes than other candidates.

AIMD analysis

Although the DFT-based calculations have provided important information about the stability of anions and binding capabilities of candidate anions with calcium ion, the behaviour of electrolytes on the anode surface is also crucial for designing better electrolytes for CIBs. AIMD simulations can probe the real-time behaviour of the electrolyte over the anode surface to unravel deep insights into the interactions. In 2021, Yamijala et al. predicted the stability of carborane-based electrolytes over Ca anode using AIMD simulations,^[9] which was later proven experimentally by Kisu et al. in the same year.^[46] In the present study, the VDE and ESW values for silaboranes show only a marginal difference from corresponding carboranes; hence, investigating their stability on the Ca anode can assist in understanding their applicability in CIBs. The DFT-based analyses reveal remarkable properties of $-\text{CF}_3$ and $-\text{NCS}$ substituted $\text{SiB}_{11}\text{H}_{12}^-$ anion. Also, the $-\text{CH}_3$ substituted $\text{SiB}_{11}\text{H}_{12}^-$ is an exciting

candidate to study the effect of incorporating an electron-donating group on the stability of calcium salt on the Ca anode. Thus, the AIMD simulations of calcium salts of silaboranes, i.e., $\text{Ca}(\text{SiB}_{11}\text{H}_{12})_2$, $\text{Ca}(\text{SiB}_{11}\text{H}_{11}\text{CF}_3)_2$, $\text{Ca}(\text{SiB}_{11}\text{H}_{11}\text{NCS})_2$ and $\text{Ca}(\text{SiB}_{11}\text{H}_{11}\text{CH}_3)_2$ salts on Ca anode were carried out and are discussed below.

The variation in the potential energy (PE) of $\text{Ca}(\text{SiB}_{11}\text{H}_{12})_2$ on the Ca anode and the charge transfer from the Ca surface to of $\text{Ca}(\text{SiB}_{11}\text{H}_{12})_2$ with time at 300 K are shown in Figure 11, along with labelled snapshots of the crucial time steps. It can be observed from the PE vs time plot given in Figure 11(a) that the PE of the system rapidly decreases in the first 0.80 ps and reaches a minimum at 0.87 ps, and then equilibrates throughout the simulation. This drastic decrease in the PE signifies breaking of Si–H bond of anion 2 (An_2) at 0.84 ps, as shown in Figure 11(c). Corresponding to the changes in PE, variation in the charges of different fragments (i.e., layer 1, layer 2, layer 3, anion 1, anion 2, and Ca^{2+}) of the system can be observed in the time-dependent charge transfer (TDCT) plots. It can be noted from Figure 11 (b) that the charge at layer 3 (Ca_L3) suddenly increases at 0.80 ps, which indicates the donation of electrons from layer 3 to the fragments over the surface. No change in the charges of anion 1 (An_1) have been observed throughout the simulation, while a steep drop can be seen in the charge of anion 2 (An_2) at 0.80 ps. This shows that An_2 accepts electrons from the Ca surface and undergoes Si–H bond breaking, whereas An_1 remains stable during the course of the dynamics. It is also interesting to note that the charge at Ca^{2+} ion decreases at the beginning of the simulation, highlighting the reduction of Ca^{2+} ion over the Ca anode surface. As there is not much interaction of layers 1 and 2 (Ca_L1 and Ca_L2) with the salt, the charges on them were almost constant throughout the simulation. The dynamics is shown in the movie S1 of the SI (cf. Section S19.1).

Further, in the simulation of $\text{Ca}(\text{SiB}_{11}\text{H}_{11}\text{CF}_3)_2$ over the Ca anode, a slight decrement in the PE (Figure 12a) is observed at 1.54 ps followed by sharp drops at 2.39, and 5.30 ps, indicating the breakage of the C–F bond (of the CF_3) in An_1, Si–C bond in An_1 and Si–C bond in An_2 (Figure 12c), respectively. The TDCT plot given in Figure 12(b) shows that in the intervals 1.30

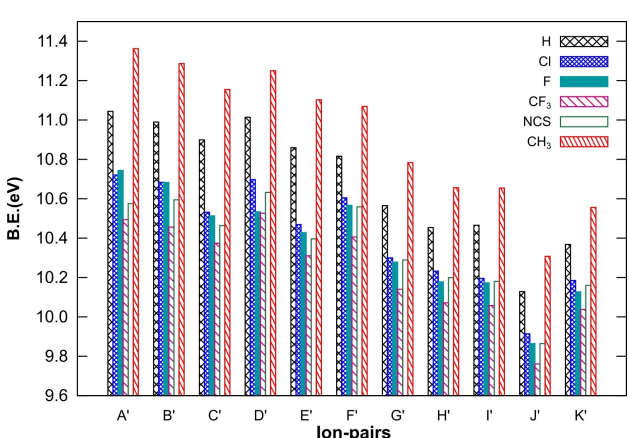


Figure 10. Variation in BE with silaborane size (where A'–K' denote the $\text{Ca}^{2+}/\text{SiB}_{n-1}\text{H}_n\text{R}^-$ ion-pairs; R = –H, –Cl, –F, –CF₃, –NCS and –CH₃; n = 5–15).

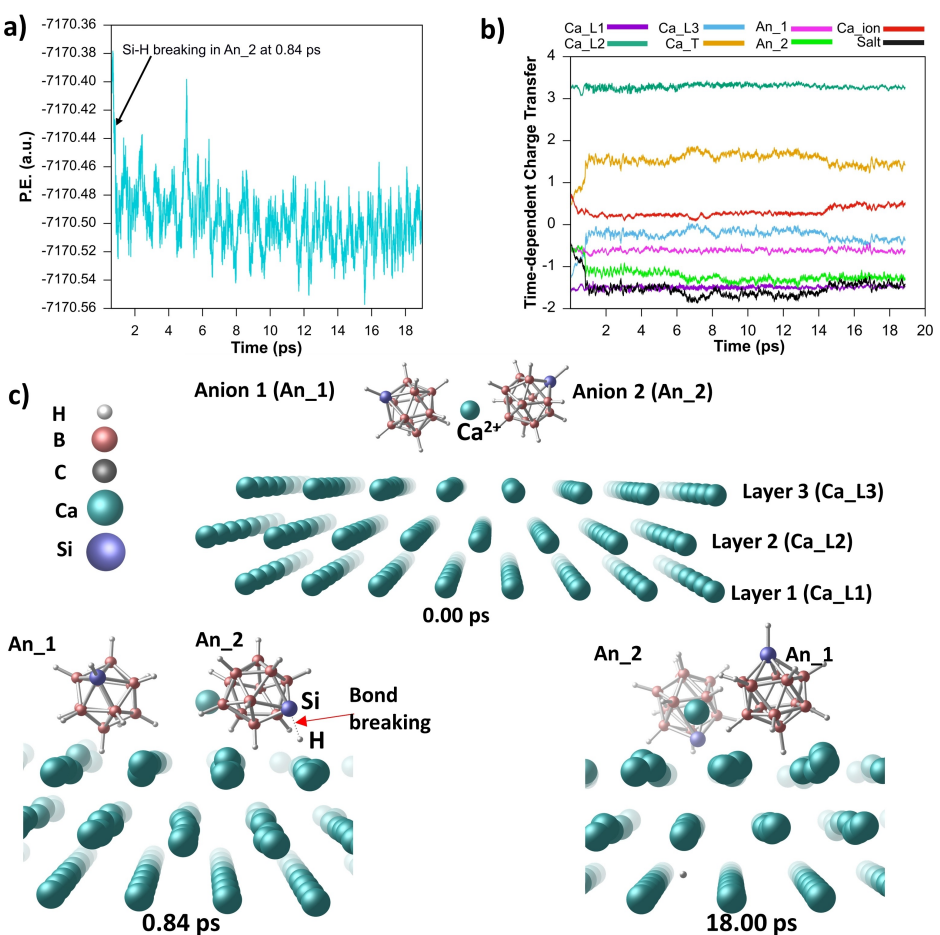


Figure 11. a) Variation in PE with time, b) charge transfer from Ca surface to $\text{Ca}(\text{SiB}_{11}\text{H}_{12})_2$ and c) snapshots at 0.00, 0.84 and 18.00 ps.

to 1.80 ps and 2.20 to 2.50 ps, the charge on An₁ abruptly decreases, signifying the acceptance of electrons from the Ca anode, while no such changes have been found in An₂ during the same interval. The An₂ fragment starts reducing at 5.30 ps of the simulation, as shown by the immediate decrease in the charge at that instant. The total charge on the Ca anode and the electrolyte salt stabilizes after 6.50 ps. It can also be noticed from the TDCT plot that the transfer of ~6 electrons takes place from the Ca anode to the salt. Also, the fluorine atoms are embedded into the Ca anode which hints at the formation of CaF_2 . Formation of CaF_2 passivation layer is a common experimental observation among the electrolytes containing F atoms in calcium-ion batteries.^[63,64] The corresponding dynamics is shown in the movie S2 of the SI (cf. section S19.2).

In the case of $\text{Ca}(\text{SiB}_{11}\text{H}_{11}\text{NCS})_2$, a drop in PE with time (Figure 13a) is observed at several intervals, which is well complemented and explained by the TDCT plots shown in Figure 13(b). Initially, an instant decrease in the charge on An₁ of $\text{Ca}(\text{SiB}_{11}\text{H}_{11}\text{NCS})_2$ can be seen at 1.30 ps showing the acceptance of electrons from the Ca surface. Then, at 1.90 ps of the simulation, An₂ starts reducing, resulting in the breakage of the Si–N bond. It is interesting to find that An₂ is getting electrons partly from the Ca surface and partly from the Ca^{2+} (Ca_{ion}), which is inferred by the increased charge of Ca^{2+} at

1.90 ps. During the breaking of the Si–N bond of An₂, the formation of $\text{Ca}^{2+}/\text{NCS}^-$ ion-pair is observed, which remains stable up to 11.58 ps and then disintegrates on the Ca surface indicated by the deflection in the PE curve. The –NCS group at An₁ starts to detach at 3.55 ps and remains stable till 4.80 ps before finally disintegrating at the Ca surface. All the critical bond breakings are shown in section S17 and the dynamics is shown in the movie S3 of the SI (cf. section S19.3). Finally, for $\text{Ca}(\text{SiB}_{11}\text{H}_{11}\text{CH}_3)_2$ salt, no sharp changes in the PE and charges (Figure 13(c) and (d)) for any fragment are observed. This shows that there is no decomposition of the $\text{Ca}(\text{SiB}_{11}\text{H}_{11}\text{CH}_3)_2$ salt on the Ca anode; thus, it remains stable throughout the simulation. Important snapshots of this simulation run are given in Figure 14. It is also noteworthy that the charge of Ca^{2+} ion decreases in the first picosecond of the simulation, showing its reduction at the anode surface. The dynamics is shown in the movie S4 of the SI (cf. Section S19.4).

Further, the variation of the distance between the calcium ion and the binding site of one of the anions in $\text{Ca}(\text{SiB}_{11}\text{H}_{11}\text{CH}_3)_2$ salt has been plotted to check the detachment of the cation from the anion (Figure S10 in Section S16 of SI). It can be seen from the plot shown in Figure S10 that the Ca^{2+} is detached from the anions after 2 ps of the simulation. Furthermore, to unravel the effect of applying external potential on stability of

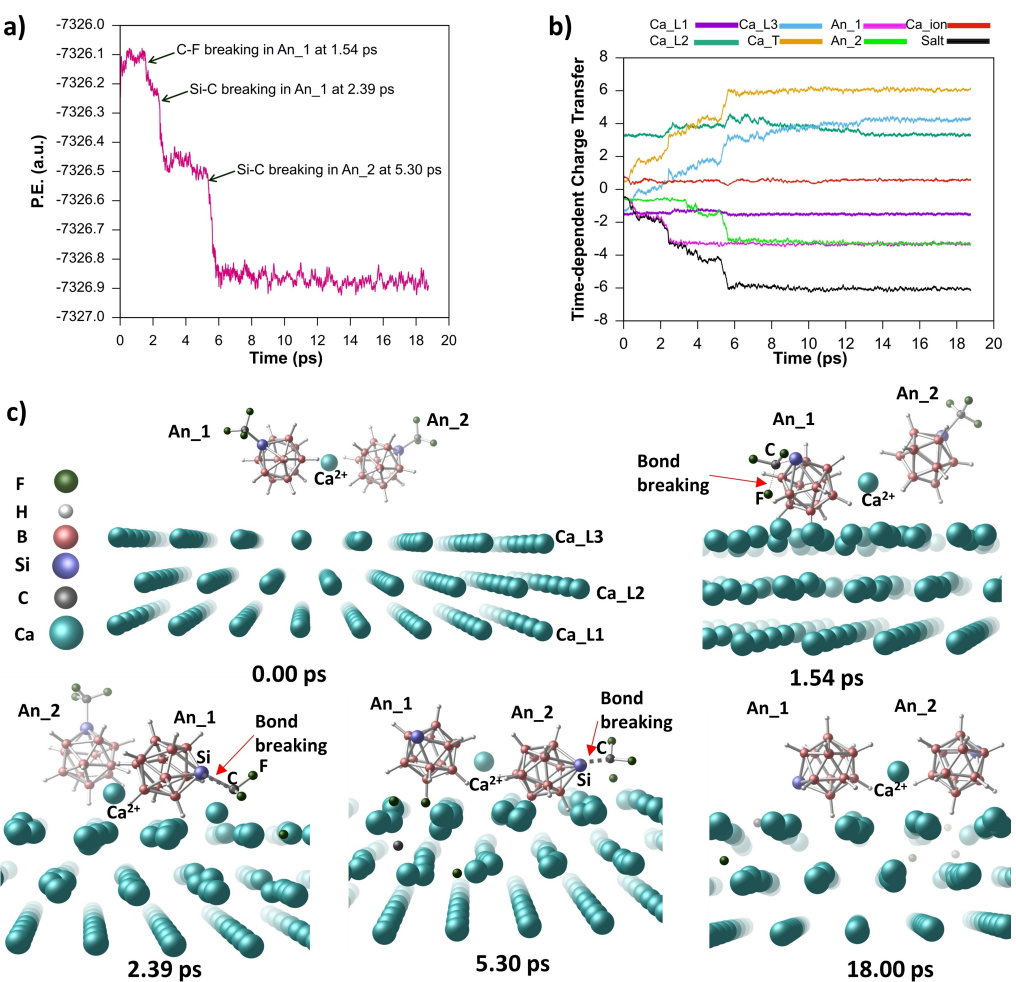


Figure 12. a) Variation in PE with time, b) charge transfer from Ca surface to $\text{Ca}(\text{SiB}_{11}\text{H}_{11}\text{CF}_3)_2$ and c) snapshots at 0.00, 1.54, 2.39, 5.30 and 18.00 ps.

$\text{Ca}(\text{SiB}_{11}\text{H}_{11}\text{CH}_3)_2$ and $\text{Ca}(\text{SiB}_{11}\text{H}_{11}\text{CF}_3)_2$ salts on Ca anode, we applied $0.2 \text{ V } \text{\AA}^{-1}$ unidirectional external electric potential on the system for 3 ps in the z-direction. It was discovered that $\text{Ca}(\text{SiB}_{11}\text{H}_{11}\text{CH}_3)_2$ was still stable while $\text{Ca}(\text{SiB}_{11}\text{H}_{11}\text{CF}_3)_2$ dissociates within 3 ps as seen in 0 V condition. This observation reflects that there is not much effect of external potential on salt stability over anode considering the gas phase calculations. However, it is noticed that the potential energy increases to higher values under the influence of $0.2 \text{ V } \text{\AA}^{-1}$ electric potential as compared to the 0 V condition (Figures S12 and S13 in SI). This increase in PE is in line with previous reports.^[65] Hence, the silaborane salts with appealing VDE, ESW, and BE values (that is, $-\text{CF}_3$, and $-\text{NCS}$ substituted) decomposed on the Ca anode highlighting the practical limitations of applications of these salts in CIBs. On the other hand, $-\text{CH}_3$ substituted silaborane salt $\text{Ca}(\text{SiB}_{11}\text{H}_{11}\text{CH}_3)_2$ remained much stable throughout the dynamics, pointing towards its potential for application in CIBs. Thus, AIMD analysis of the unexplored salts of silaboranes unveils interesting facts about their stability at the Ca anode, which can help to design future silaborane-based electrolytes for CIBs.

Furthermore, to shed more light on the practical applications of the $\text{SiB}_{11}\text{H}_{11}\text{CH}_3^-$ ion (which shows highest stability on

Ca anode) based electrolytes in CIBs, we computed the anodic stability of $\text{SiB}_{11}\text{H}_{11}\text{CH}_3^-$ anion. To calculate the anodic stability (oxidation potential), we used the prominent thermodynamic cycle-based approach as described in the work of Persson and co-workers.^[66] To ensure the reliability of the computational methods employed, we first computed the anodic stability of the widely studied $\text{CB}_{11}\text{H}_{12}^-$ ion. In 2018, Nathan et al. investigated the stability of carba-closo-dodecaborate ($\text{CB}_{11}\text{H}_{12}^-$) anion for high voltage battery electrolytes in magnesium-ion batteries.^[59] The authors reported that the experimental anodic stability of $\text{CB}_{11}\text{H}_{12}^-$ ion is 4.6 V vs. $\text{Mg}^{0/2+}$. The theoretically calculated anodic stability for $\text{CB}_{11}\text{H}_{12}^-$ ion was reported to be 4.89 V vs. $\text{Mg}^{0/2+}$ which is slightly higher than the experimentally observed value. Hence, we computed the anodic stability of $\text{CB}_{11}\text{H}_{12}^-$ ion which was found to be 4.9 V vs. $\text{Mg}^{0/2+}$ ion and this value is very close to the experimental and theoretical values reported by Nathan et al.^[59] After validating the suitability of our computational methodology to reproduce experimental results, we computed the anodic stability of the most promising electrolyte in our AIMD simulation run i.e., $\text{SiB}_{11}\text{H}_{11}\text{CH}_3^-$ ion. The calculated oxidation potential for $\text{SiB}_{11}\text{H}_{11}\text{CH}_3^-$ is found to be 5.5 V vs. Ca/Ca^{2+} . The calculated value is expected to be slightly overestimated than

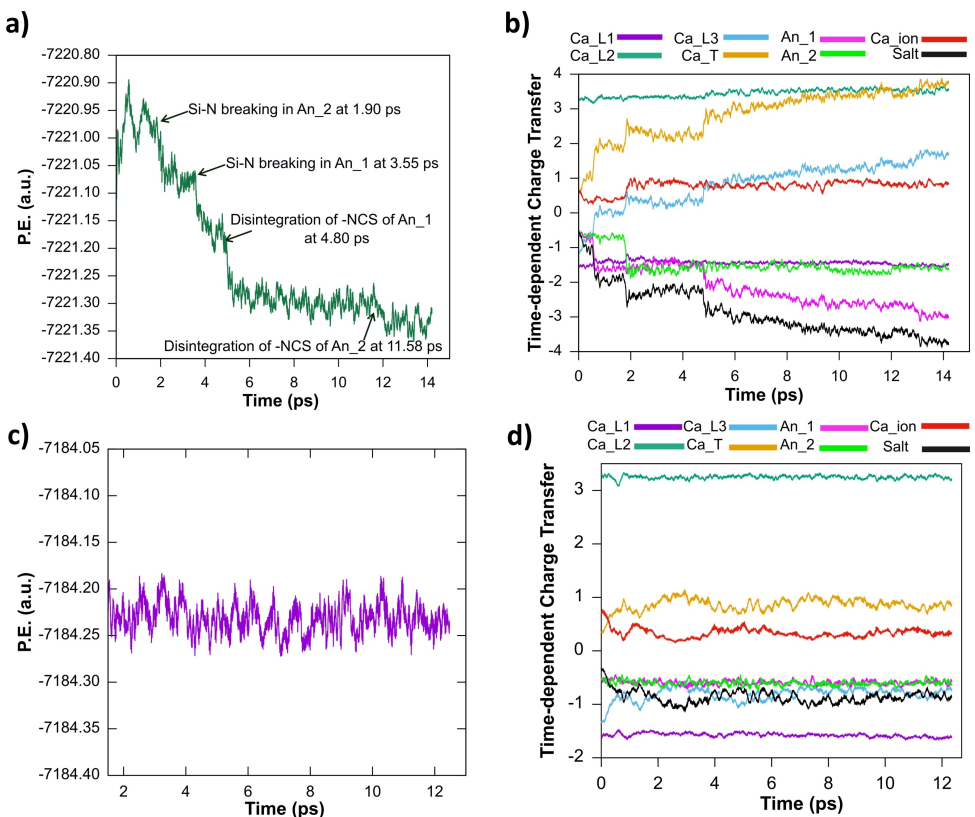


Figure 13. Variation in PE with time for a) $\text{Ca}(\text{SiB}_{11}\text{H}_{11}\text{NCS})_2$ and c) $\text{Ca}(\text{SiB}_{11}\text{H}_{11}\text{CH}_3)_2$, and TDCT plots for b) $\text{Ca}(\text{SiB}_{11}\text{H}_{11}\text{NCS})_2$ and d) $\text{Ca}(\text{SiB}_{11}\text{H}_{11}\text{CH}_3)_2$.

in real experiments. However, this value of anodic potential signifies that $\text{SiB}_{11}\text{H}_{11}\text{CH}_3^-$ based calcium salts may be a suitable electrolyte for the CIBs and hence calls for experimental investigations. It is noteworthy that the $\text{SiB}_{11}\text{H}_{11}\text{CH}_3^-$ ion was successfully synthesized in 1996 by Wesemann et al.^[67] Several salts based on carborane clusters are already reported in literature such as $\text{Ca}(\text{CB}_{11}\text{H}_{12})_2$, $\text{Mg}(\text{CB}_{11}\text{H}_{12})_2$, $\text{Zn}(\text{CB}_{11}\text{H}_{12})_2$, and $\text{Mg}(\text{CB}_9\text{H}_{10})_2$ where they have been experimentally synthesized and investigated for application in different batteries.^[45,46,68] This highlights the experimental feasibility of the synthesis of $\text{Ca}(\text{SiB}_{11}\text{H}_{11}\text{CH}_3)_2$ salt. Therefore, the applica-

tion of $\text{Ca}(\text{SiB}_{11}\text{H}_{11}\text{CH}_3)_2$ based electrolytes in non-aqueous CIBs may prove to be highly promising.

Conclusions

In this work, we have successfully investigated the potential of less explored silaborane-based electrolytes for application in next-generation Ca-ion batteries. More specifically, we have examined the stability of silaboranes in terms of vertical detachment energies and the electrochemical stability win-

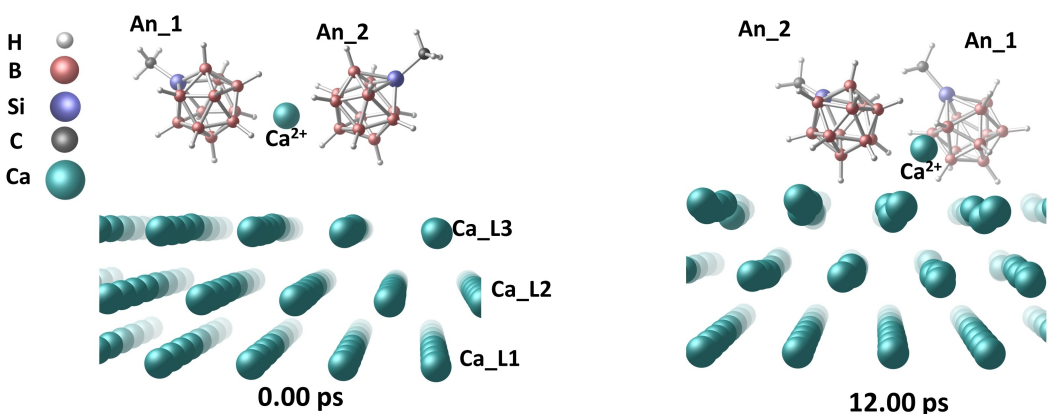


Figure 14. Snapshots of important time steps in the simulation of $\text{Ca}(\text{SiB}_{11}\text{H}_{11}\text{CH}_3)_2$ at 0.00 ps and 12.00 ps.

dows. The VDE analysis shows that the $\text{SiB}_{11}\text{H}_{12}^-$ anion possesses the maximum VDE among the unsubstituted silaboranes. Such high VDE of $\text{SiB}_{11}\text{H}_{12}^-$ anion is a consequence of its high symmetry and extensive 3-dimensional aromatization. Similar trends are obtained for ESWs of silaboranes, where the $\text{SiB}_{11}\text{H}_{12}^-$ anion displays the highest ESW value. Besides VDE and ESW, another crucial parameter, binding energy, was also computed for all structures. An MESP surface analysis-based method was developed, which successfully predicts the most probable binding site for cation on the cluster anions.

To get silaboranes with better properties, their functionalization was done. In most cases, the $-\text{CF}_3$ and $-\text{NCS}$ substitution shows maximum increment in VDEs and ESWs of silaboranes besides decreasing the binding energies. The $-\text{CF}_3$ and $-\text{NCS}$ substituted $\text{SiB}_{11}\text{H}_{12}^-$ ion displays better properties than other silaboranes. Further, $\text{Ca}(\text{SiB}_{11}\text{H}_{11}\text{R})_2$ salts ($\text{R} = \text{H}$, $-\text{CF}_3$, $-\text{NCS}$, $-\text{CH}_3$) were subjected to AIMD on the Ca anode. Interestingly, most of the Ca salts such as $\text{Ca}(\text{SiB}_{11}\text{H}_{12})_2$, $\text{Ca}(\text{SiB}_{11}\text{H}_{11}\text{NCS})_2$ and $\text{Ca}(\text{SiB}_{11}\text{H}_{11}\text{CF}_3)_2$, decompose on the calcium anode. On the contrary, $\text{Ca}(\text{SiB}_{11}\text{H}_{11}\text{CH}_3)_2$ remains stable on the Ca anode throughout the dynamics. Therefore, we conclude that silaboranes can also be used for application in CIBs with appropriate functionalization. The $\text{Ca}(\text{SiB}_{11}\text{H}_{11}\text{CH}_3)_2$ salt appears to be a good electrolyte for practical CIBs. We discourage the use of the $-\text{CF}_3$ functional group due to the prominent passivation issue associated with fluorine, as also evident from AIMD simulation. The DFT and AIMD studies highlight that the stability of the electrolyte, both as an individual moiety and its stability on the anode, is essential for predicting better electrolytes. Further, the functionalized anions constituting electrolytes with enhanced properties may not necessarily be stable on the anode. Our work will aid in the development of better electrolytes for CIBs and encourage experimentalists to synthesize and investigate silaborane-based Ca salts for application in CIBs.

Computational Methods

DFT Calculations

The structures of the considered anions (carboranes and silaboranes) were fully optimized at $\omega\text{B97XD3}/6-311+\text{G}(\text{d},\text{p})$ level of theory without any geometrical and symmetrical constraints. The ωB97XD3 functional is a range-separated hybrid functional that includes long as well as short-range interactions.^[69] To benchmark our computational method, we have systematically compared the important bond lengths and bond angles in our computational model of $-\text{CH}_3$ substituted $\text{SiB}_{11}\text{H}_{12}^-$ and $\text{CB}_{11}\text{H}_{12}^-$ anions with the experimentally reported crystal structures of these anions.^[67,70] The comparison is shown in the tables under Section S2. From the Tables S1 and S2, it can be observed that the computed bond lengths and angles are in outstanding agreement with the experimental data, showcasing the effectiveness of the computational method used here for boron-based clusters. All the DFT calculations were carried out using the latest ORCA 5.0.3 program

package.^[71] The RIJCOSX (Resolution-of-the-identity for Coulomb with a chain of sphere algorithm for the Hartree-Fock exchange part) approximation was used to step up the calculations.^[72] The vibrational analyses were also conducted to confirm the optimized structures as local minima. Also, the charge possessed by each atom was computed using the natural population analysis (NPA), which is based on the natural bond orbitals (NBO) employing JANPA.^[73,74] The molecular electrostatic potential (MESP) surface analysis for the candidate anions was also done at an isovalue of 0.001 a.u. using the Multiwfn code.^[75] The overall charge of the system of cluster anion and calcium ion is +1 such that formal charge of Ca is +2 while the anion possesses a formal charge of -1.

The optimized structures of the anions were used for calculating the VDE, ESW, and BE. The VDE is determined by taking the difference between the energies of the anion and the corresponding neutral species possessing the anion geometry, as shown in equation 1.^[4,57,60]

$$\text{VDE} = E[\text{XB}_{n-1}\text{H}_n]_{\text{single point}} - E[\text{XB}_{n-1}\text{H}_n^-]_{\text{optimized}} \quad (1)$$

where, $E[\text{XB}_{n-1}\text{H}_n^-]_{\text{optimized}}$ is the energy of the optimized anion while $E[\text{XB}_{n-1}\text{H}_n]_{\text{single point}}$ denotes the single point energy of the same anion with one electron less. The single point energy of the neutral species corresponding to the respective anions was also calculated at the same level of theory. Further, the nuclear independent chemical shift (NICS) values at the geometrical centres of the anions were calculated using Schleyer and co-worker's formalism^[76] employing the NMR module available in ORCA.

To evaluate ESWs, the frontier molecular orbitals-based approach was used, according to which the cathodic limit (V_{CL}) and the anodic limit (V_{AL}) are set by the energies of the lowest unoccupied molecular orbital (LUMO) and highest occupied molecular orbital (HOMO) respectively.^[77,78] The ESW is then calculated by taking the difference between V_{CL} and V_{AL} . This method works well for rapid screening where only the trend prediction is required rather than the absolute values.^[77] It is helpful for initial screening of the electrolytes to get idea about their stability as individual moieties. However, other aspects of stability are also important such as stability of electrolytes on metal anode which we investigated using AIMD simulations.

For one electron transfer, the ESWs of all candidate anions are calculated using the following equations.

$$V_{\text{CL}} = \frac{-E_{\text{LUMO}}}{e} \quad (2)$$

and,

$$V_{\text{AL}} = \frac{-E_{\text{HOMO}}}{e} \quad (3)$$

The binding energy is the energy required to separate the metal cation from the anion and is expressed as

$$\Delta E_{\text{Ca}^{2+}} = (E_{\text{Ca}^{2+}} + E_{\text{anion}}) - E_{\text{ion-pair}} \quad (4)$$

where, $\Delta E_{\text{Ca}^{2+}}$ represents the BE of Ca^{2+} and cluster anion, $E_{\text{Ca}^{2+}}$, E_{anion} , $E_{\text{ion-pair}}$ are the energies of the Ca^{2+} ion, anion, and ion-pair, respectively. All calculations were performed in the gaseous phase.

Further, to verify the predictions made by above mentioned gas phase calculations, we calculated the BEs of the unsubstituted silaboranes and functionalized silaboranes ($\text{SiB}_{11}\text{H}_{11}\text{R}^-$; $\text{R}=\text{NCS}$, $-\text{CF}_3$, $-\text{F}$, $-\text{Cl}$, and $-\text{CH}_3$) in the presence of two different solvents, i.e., tetrahydrofuran (THF) and dimethoxyethane (DME) using an implicit solvation model (conductor-like polarizable continuum model (CPCM)). The BEs of the functionalized silaboranes ($\text{SiB}_{11}\text{H}_{11}\text{R}^-$; $\text{R}=\text{NCS}$, $-\text{CF}_3$, $-\text{F}$, $-\text{Cl}$, and $-\text{CH}_3$) were also calculated in the presence of one THF or one DME molecule to mimic the effect of explicit solvation shell. All the calculated BEs using implicit and explicit solvation models were systematically compared with the gas phase BEs and the correlation plots between the BEs in gas phase and in implicit/explicit solvents are given along with detailed discussion in the SI under Section S14. From the correlation plots, it is clear that the trends predicted by the gas phase calculations remain the same in the presence of solvent models (implicit and explicit both). Such observations have been reported in literature for other properties also (for instance, ionization potentials^[79]). These calculations indicate that the employed technique to screen the proposed anions is adequate enough to give reliable results since relative chemical trends were found to be the same in presence and absence of solvation model. Furthermore, the BEs of Ca^{2+} ion with TFSI^- , ClO_4^- , and BF_4^- were also calculated in gas phase as well as using implicit solvation model (THF). Calcium salts of these anions are already reported in previous works.^[32,63,64] We calculated and compared the BEs of $\text{Ca}^{2+}/\text{SiB}_{11}\text{H}_{11}\text{CH}_3^-$ ion pair (found most suitable in our analysis) with $\text{Ca}^{2+}/\text{ClO}_4^-$, $\text{Ca}^{2+}/\text{TFSI}^-$, and $\text{Ca}^{2+}/\text{BF}_4^-$ ion pairs. The calculated BEs are provided in Table S10 in the SI (Section S13). The comparison of BEs of Ca^{2+} with TFSI^- , ClO_4^- , BF_4^- and $\text{SiB}_{11}\text{H}_{11}\text{CH}_3^-$ anion shows that $\text{SiB}_{11}\text{H}_{11}\text{CH}_3^-$ binds less firmly to the Ca^{2+} ion than other counter anions pointing towards its possible implementation to develop better CIBs.

AIMD simulations

The potential calcium salts of silaboranes were then subjected to *ab initio* molecular dynamics (AIMD). The Ca salts of silaboranes were first optimized using ORCA 5.0.3 program. The salts were then placed over the Ca anode surface and re-optimized using CP2K software. Further dynamical calculations were also carried out using CP2K.^[80] The details related to the construction of the Ca anode surface model are provided in Section S1 of the SI. The anode slab was constructed using the Ca unit cell provided by the Materials Project database.^[81] The fully optimized structure of the salt over the anode surface was taken as the initial geometry for the AIMD simulation. The DZVP-MOLOPT basis set along with Goedecker-Teter-Hutter

(GTH)^[82,83] pseudopotential, PBE (Perdew-Burke-Ernzerhof) functional,^[84] and Grimme's D3 dispersion correction was used for the simulations.^[85,86] The plane-wave energy and reference grid cut-offs were set to 300 and 60 Ry, respectively for the auxiliary plane-wave basis. The optimization calculations were converged when the force on every atom was less than $0.02 \text{ eV}\text{\AA}^{-1}$. The Nose-Hoover thermostat with a 3-chain length was utilized to maintain the temperature at 300 K. A timestep of 1 fs was used for the numerical integrations, and a canonical ensemble (NVT) was employed to carry out the simulations. Also, the Mulliken charges produced at each time step were considered for time-dependent charge-transfer investigations. All the molecular graphics were generated using CYLview.^[87]

Supporting Information

Additional references cited within the Supporting Information.^[59,79,81]

Acknowledgements

AS thanks Ministry of Education (MoE) for fellowship and PG acknowledges Science and Engineering Research Board (SERB) (CRG/2021/000759) for financial assistance. AT acknowledges PMRF (PM-31-22-618-414) for financial support. The authors gratefully acknowledge the National Supercomputing Mission (NSM) for providing computing resources of 'PARAM Ganga' at the Indian Institute of Technology Roorkee, which is implemented by C-DAC and supported by the Ministry of Electronics and Information Technology (MeitY) and Department of Science and Technology (DST), Government of India. We would like to thank Dr. Ashu Choudhary (Department of Chemical Engineering, IIT Roorkee) for suggestions and helpful discussions.

Conflict of Interests

The authors declare no conflict of interest.

Data Availability Statement

The data that support the findings of this study are available in the supplementary material of this article.

Keywords: *Ab initio* molecular dynamics • calcium-ion batteries • density functional theory • silaboranes • time-dependent charge transfer

- [1] M. S. Whittingham, *Chem. Rev.* **2004**, *104*, 4271–4302.
- [2] H. Liu, X. Liu, W. Li, X. Guo, Y. Wang, G. Wang, D. Zhao, *Adv. Energy Mater.* **2017**, *7*, 1700283.
- [3] A. L. Santhosha, L. Medenbach, J. R. Buchheim, P. Adelhelm, *Batteries Supercaps* **2019**, *2*, 524–529.

- [4] A. K. Kushwaha, S. S. Jena, P. Jena, S. K. Nayak, *J. Phys. Chem. C* **2022**, *126*, 5112–5121.
- [5] Y. Li, S. Guan, H. Huo, Y. Ma, Y. Gao, P. Zuo, G. Yin, *Adv. Funct. Mater.* **2021**, *31*, 2100650.
- [6] I. D. Hosein, *ACS Energy Lett.* **2021**, *6*, 1560–1565.
- [7] M. Rashad, M. Asif, Y. Wang, Z. He, I. Ahmed, *Energy Storage Mater.* **2020**, *25*, 342–375.
- [8] J. Park, Z. Xu, G. Yoon, S. K. Park, J. Wang, H. Hyun, H. Park, J. Lim, Y. Ko, Y. S. Yun, K. Kang, *Adv. Mater.* **2020**, *32*, 1904411.
- [9] S. S. R. K. C. Yamjala, H. Kwon, J. Guo, B. M. Wong, *ACS Appl. Mater. Interfaces* **2021**, *13*, 13114–13122.
- [10] B. Ji, H. He, W. Yao, Y. Tang, *Adv. Mater.* **2021**, *33*, 2005501.
- [11] M. Song, H. Tan, D. Chao, H. J. Fan, *Adv. Funct. Mater.* **2018**, *28*, 1802564.
- [12] X. Zheng, T. Ahmad, W. Chen, *Energy Storage Mater.* **2021**, *39*, 365–394.
- [13] M.-C. Lin, M. Gong, B. Lu, Y. Wu, D.-Y. Wang, M. Guan, M. Angell, C. Chen, J. Yang, B.-J. Hwang, H. Dai, *Nature* **2015**, *520*, 324–328.
- [14] A. V. G. S. B. Mishra, S. Ramaprabhu, B. R. K. Nanda, *Nanoscale Adv.* **2022**, *4*, 3870–3882.
- [15] K. Ta, R. Zhang, M. Shin, R. T. Rooney, E. K. Neumann, A. A. Gewirth, *ACS Appl. Mater. Interfaces* **2019**, *11*, 21536–21542.
- [16] Y. Jie, Y. Tan, L. Li, Y. Han, S. Xu, Z. Zhao, R. Cao, X. Ren, F. Huang, Z. Lei, G. Tao, G. Zhang, S. Jiao, *Angew. Chem. Int. Ed.* **2020**, *59*, 12689–12693.
- [17] X. Jiao, X. Pan, *J. Electroanal. Chem.* **2021**, *882*, 114995.
- [18] J. B. Moss, L. Zhang, K. V. Nielson, Y. Bi, C. Wu, S. Scheiner, T. L. Liu, *Batteries Supercaps* **2019**, *2*, 792–800.
- [19] J. D. Forero-Saboya, D. S. Tchitchekova, P. Johansson, M. R. Palacín, A. Ponrouch, *Adv. Mater. Interfaces* **2022**, *9*, 2101578.
- [20] Y. Liang, H. Dong, D. Aurbach, Y. Yao, *Nat. Energy* **2020**, *5*, 646–656.
- [21] D. Monti, A. Ponrouch, R. B. Araujo, F. Barde, P. Johansson, M. R. Palacín, *Front. Chem.* **2019**, *7*, 79.
- [22] M. E. Arroyo-de Dompablo, A. Ponrouch, P. Johansson, M. R. Palacín, *Chem. Rev.* **2020**, *120*, 6331–6357.
- [23] A. M. Melemed, A. Khurram, B. M. Gallant, *Batteries Supercaps* **2020**, *3*, 570–580.
- [24] D. Aurbach, R. Skaletsky, Y. Gofer, *J. Electrochem. Soc.* **1991**, *138*, 3536–3545.
- [25] J. Forero-Saboya, C. Davoisne, R. Dedryvère, I. Yousef, P. Canepa, A. Ponrouch, *Energy Environ. Sci.* **2020**, *13*, 3423–3431.
- [26] A. Shyamsunder, L. E. Blanc, A. Assoud, L. F. Nazar, *ACS Energy Lett.* **2019**, *4*, 2271–2276.
- [27] R. B. Araujo, V. Thangavel, P. Johansson, *Energy Storage Mater.* **2021**, *39*, 89–95.
- [28] Q. Wei, L. Zhang, X. Sun, T. L. Liu, *Chem. Sci.* **2022**, *13*, 5797–5812.
- [29] A. Meitav, E. Peled, *J. Electrochem. Soc.* **1981**, *128*, 825–831.
- [30] E. Peled, A. Meitav, M. Brand, *J. Electrochem. Soc.* **1981**, *128*, 1936–1938.
- [31] R. J. Staniewicz, *J. Electrochem. Soc.* **1980**, *127*, 782.
- [32] A. Ponrouch, C. Frontera, F. Bardé, M. R. Palacín, *Nat. Mater.* **2016**, *15*, 169–172.
- [33] R. Zhou, Z. Hou, Q. Liu, X. Du, J. Huang, B. Zhang, *Adv. Funct. Mater.* **2022**, *32*, 2200929.
- [34] P.-A. Martin, F. Årén, P. Johansson, *Batteries Supercaps* **2023**, DOI:10.1002/batt.202300003.
- [35] Z. Li, O. Fuhr, M. Fichtner, Z. Zhao-Karger, *Energy Environ. Sci.* **2019**, *12*, 3496–3501.
- [36] I. Krossing, A. Reisinger, *Coord. Chem. Rev.* **2006**, *250*, 2721–2744.
- [37] I. M. Riddlestone, A. Kraft, J. Schaefer, I. Krossing, *Angew. Chem. Int. Ed.* **2018**, *57*, 13982–14024.
- [38] S. Kim, H. Oguchi, N. Toyama, T. Sato, S. Takagi, T. Otomo, D. Arunkumar, N. Kuwata, J. Kawamura, S. Orimo, *Nat. Commun.* **2019**, *10*, 1081.
- [39] W. S. Tang, M. Matsuo, H. Wu, V. Stavila, W. Zhou, A. A. Talin, A. V. Solonin, R. V. Skoryunov, O. A. Babanova, A. V. Skripov, A. Unemoto, S. Orimo, T. J. Udvovic, *Adv. Energy Mater.* **2016**, *6*, 1502237.
- [40] R. Mohtadi, S. Orimo, *Nat. Rev. Mater.* **2017**, *2*, 16091.
- [41] O. Tutusaus, R. Mohtadi, T. S. Arthur, F. Mizuno, E. G. Nelson, Y. V. Sevryugina, *Angew. Chem. Int. Ed.* **2015**, *54*, 7900–7904.
- [42] H. Dong, O. Tutusaus, Y. Liang, Y. Zhang, Z. Lebens-Higgins, W. Yang, R. Mohtadi, Y. Yao, *Nat. Energy* **2020**, *5*, 1043–1050.
- [43] R. Mohtadi, A. Remhof, P. Jena, *J. Phys. Condens. Matter* **2016**, *28*, 353001.
- [44] S. Giri, S. Behera, P. Jena, *Angew. Chem. Int. Ed.* **2014**, *53*, 13916–13919.
- [45] A. Berger, A. Ibrahim, C. E. Buckley, M. Paskevicius, *Phys. Chem. Chem. Phys.* **2023**, *25*, 5758–5775.
- [46] K. Kisu, S. Kim, T. Shinohara, K. Zhao, A. Züttel, S. Orimo, *Sci. Rep.* **2021**, *11*, 7563.
- [47] Y.-Y. Sun, J.-F. Li, F.-Q. Zhou, J.-L. Li, B. Yin, *Phys. Chem. Chem. Phys.* **2016**, *18*, 28576–28584.
- [48] D. Liepinya, M. Smeu, *Energy Mater. Adv.* **2021**, *2021*, 2021–9769347.
- [49] H. Jeong, E. P. Kamphaus, P. C. Redfern, N. T. Hahn, N. J. Leon, C. Liao, L. Cheng, *ACS Appl. Mater. Interfaces* **2023**, *15*, 6933–6941.
- [50] S. Pathreker, I. D. Hosein, *Why Is Tetrahydrofuran a Good Solvent for Calcium Batteries? Insights From Ab Initio Molecular Dynamics Simulations*, *Chemistry*, **2021**.
- [51] J. Young, M. Smeu, *Adv. Theory Simul.* **2021**, *4*, 2100018.
- [52] J. Young, P. M. Kulick, T. R. Juran, M. Smeu, *ACS Appl. Energy Mater.* **2019**, *2*, 1676–1684.
- [53] J. Young, M. Smeu, *J. Phys. Chem. Lett.* **2018**, *9*, 3295–3300.
- [54] P. von R. Schleyer, K. Najafian, *Inorg. Chem.* **1998**, *37*, 3454–3470.
- [55] M. Zhong, J. Zhou, H. Fang, P. Jena, *Phys. Chem. Chem. Phys.* **2017**, *19*, 17937–17943.
- [56] H. Fang, P. Jena, *J. Phys. Chem. C* **2017**, *121*, 7697–7702.
- [57] A. K. Srivastava, N. Misra, *Polyhedron* **2016**, *117*, 422–426.
- [58] C. Sikorska, *ChemPhysChem* **2019**, *20*, 2236–2246.
- [59] N. T. Hahn, T. J. Seguin, K.-C. Lau, C. Liao, B. J. Ingram, K. A. Persson, K. R. Zavadil, *J. Am. Chem. Soc.* **2018**, *140*, 11076–11084.
- [60] S. Sinha, P. Jena, S. Giri, *Phys. Chem. Chem. Phys.* **2022**, *24*, 21105–21111.
- [61] J. B. Goodenough, Y. Kim, *Chem. Mater.* **2010**, *22*, 587–603.
- [62] S. Körbe, P. J. Schreiber, J. Michl, *Chem. Rev.* **2006**, *106*, 5208–5249.
- [63] Z. Hou, R. Zhou, Y. Yao, Z. Min, Z. Lu, Y. Zhu, J. Tarascon, B. Zhang, *Angew. Chem. Int. Ed.* **2022**, *61*, DOI: 10.1002/anie.202214796.
- [64] C. Bodin, J. Forero Saboya, P. Jankowski, K. Radan, D. Foix, C. Courrèges, I. Yousef, R. Dedryvère, C. Davoisne, M. Lozinšek, A. Ponrouch, *Batteries Supercaps* **2023**, *6*, e202200433.
- [65] V. Ponce, D. E. Galvez-Aranda, J. M. Seminario, *J. Phys. Chem. C* **2017**, *121*, 12959–12971.
- [66] L. Cheng, R. S. Assary, X. Qu, A. Jain, S. P. Ong, N. N. Rajput, K. Persson, L. A. Curtiss, *J. Phys. Chem. Lett.* **2015**, *6*, 283–291.
- [67] L. Wesemann, U. Englert, *Angew. Chem. Int. Ed. Engl.* **1996**, *35*, 527–527.
- [68] S. G. McArthur, R. Jay, L. Geng, J. Guo, V. Lavallo, *Chem. Commun.* **2017**, *53*, 4453–4456.
- [69] Y.-S. Lin, G.-D. Li, S.-P. Mao, J.-D. Chai, *J. Chem. Theory Comput.* **2013**, *9*, 263–272.
- [70] K. Shelly, D. C. Finster, Y. J. Lee, W. R. Scheidt, C. A. Reed, *J. Am. Chem. Soc.* **1985**, *107*, 5955–5959.
- [71] F. Neese, *Wiley Interdiscip. Rev. Comput. Mol. Sci.* **2022**, *12*, e1606.
- [72] S. Kossmann, F. Neese, *J. Chem. Theory Comput.* **2010**, *6*, 2325–2338.
- [73] T. Y. Nikolaienko, L. A. Bulavin, D. M. Horovun, *Comput. Theor. Chem.* **2014**, *1050*, 15–22.
- [74] T. Y. Nikolaienko, L. A. Bulavin, *Int. J. Quantum Chem.* **2019**, *119*, e25798.
- [75] T. Lu, F. Chen, *J. Comput. Chem.* **2012**, *33*, 580–592.
- [76] P. von R. Schleyer, C. Maerker, A. Dransfeld, H. Jiao, N. J. R. van Eikema Hommes, *J. Am. Chem. Soc.* **1996**, *118*, 6317–6318.
- [77] S. Kazemabnabi, Z. Zhang, K. Thornton, S. Banerjee, *J. Phys. Chem. B* **2016**, *120*, 5691–5702.
- [78] S. P. Ong, O. Andreussi, Y. Wu, N. Marzari, G. Ceder, *Chem. Mater.* **2011**, *23*, 2979–2986.
- [79] N. N. Rajput, X. Qu, N. Sa, A. K. Burrell, K. A. Persson, *J. Am. Chem. Soc.* **2015**, *137*, 3411–3420.
- [80] J. Vande Vondele, M. Krack, F. Mohamed, M. Parrinello, T. Chassaing, J. Hutter, *Comput. Phys. Commun.* **2005**, *167*, 103–128.
- [81] *The Materials Project. Materials Data on Ca by Materials Project*. United States: N.p. **2020**. DOI:10.17188/1208213.
- [82] S. Goedecker, M. Teter, J. Hutter, *Phys. Rev. B* **1996**, *54*, 1703–1710.
- [83] M. Krack, *Theor. Chem. Acc.* **2005**, *114*, 145–152.
- [84] J. P. Perdew, K. Burke, M. Ernzerhof, *Phys. Rev. Lett.* **1996**, *77*, 3865–3868.
- [85] S. Grimme, J. Antony, S. Ehrlich, H. Krieg, *J. Chem. Phys.* **2010**, *132*, 154104.
- [86] S. Grimme, S. Ehrlich, L. Goerigk, *J. Comput. Chem.* **2011**, *32*, 1456–1465.
- [87] C. Legault, *Univ. Sherbrooke* **2009**, *436*, 437.

Manuscript received: February 27, 2023

Revised manuscript received: June 15, 2023

Accepted manuscript online: June 15, 2023

Version of record online: July 11, 2023